JACS
JOURNAL OF THE AMERICAN CHEMICAL SOCIETY

Article

pubs.acs.org/JACS

Molecular Interactions between Graphene and Biological Molecules

Xingquan Zou,[†,§] Shuai Wei,[†,§] Joshua Jasensky,[†] Minyu Xiao,[†] Qiuming Wang,[†] Charles L. Brooks III,[*,†,‡] and Zhan Chen[*,†,‡]

[†]Department of Chemistry, and [‡]Department of Biophysics, University of Michigan, Ann Arbor, Michigan 48109, United States

Supporting Information

ABSTRACT: Applications of graphene have extended into areas of nanobio-technology such as nanobio-medicine, nanobio-sensing, as well as nanoelectronics with biomolecules. These applications involve interactions between proteins, peptides, DNA, RNA etc. and graphene, therefore understanding such molecular interactions is essential. For example, many applications based on using graphene and peptides require peptides to interact with (e.g., noncovalently bind to) graphene at one end, while simultaneously exposing the other end to the surrounding medium (e.g., to detect analytes in solution). To control and characterize peptide behavior on a graphene surface in solution is difficult. Here we successfully probed the molecular interactions between two peptides (cecropin P1 and MSI-78(C1)) and graphene in situ and in real-time using sum frequency generation (SFG) vibrational spectroscopy and molecular dynamics (MD) simulation. We demonstrated that the distribution of various planar (including aromatic (Phe, Trp, Tyr, and His)/amide (Asn and Gln)/Guanidine (Arg)) side-chains and charged hydrophilic (such as Lys) side-chains in a peptide sequence determines the orientation of the peptide adsorbed on a graphene surface. It was found that peptide interactions with graphene depend on the competition between both planar and hydrophilic residues in the peptide. Our results indicated that part of cecropin P1 stands up on graphene due to an unbalanced distribution of planar and hydrophilic residues, whereas MSI-78(C1) lies down on graphene due to an even distribution of Phe residues and hydrophilic residues. With such knowledge, we could rationally design peptides with desired residues to manipulate peptide−graphene interactions, which allows peptides to adopt optimized structure and exhibit excellent activity for nanobio-technological applications. This research again demonstrates the power to combine SFG vibrational spectroscopy and MD simulation in studying interfacial biological molecules.

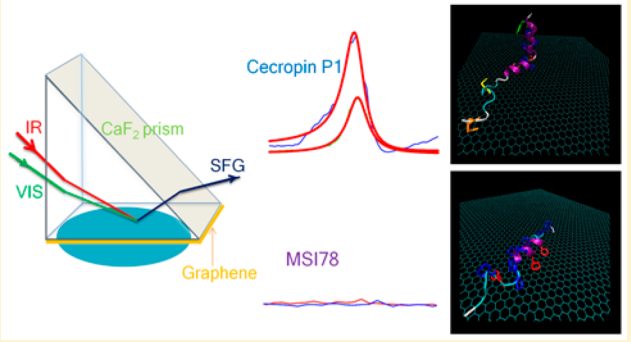

1. INTRODUCTION

Graphene, a two-dimensional (2D) sp2-hybridized carbon material, has been extensively studied due to its fascinating properties and potential applications.[1,2] Recently, applications of graphene have been expanded to nanobio-medicine and nanobio-sensing.[3−6] The large 2D aromatic surface of graphene makes it an ideal substrate for immobilization of biomolecules via their $\pi-\pi$ stacking interaction. Many applications take advantage of the noncovalent interface functionalization to preserve the intrinsic properties of graphene.[7−14] Graphene-based biosensing applications mostly depend on conductivity changes in graphene as a result of analyte adsorption creating local electronic doping.[7] Khatayevich et al.[15] have demonstrated the selective detection of target proteins by a peptide-enabled graphene biosensor, which can detect streptavidin against a background of serum bovine albumin at less than 50 ng/mL. Ohno et al.[4] have reported a label-free immunosensor based on a peptide aptamer-modified graphene field-effect transistor (G-FET). The aptamer-modified G-FET showed selective electrical detection of IgE protein, whereas other proteins were not detected. From the dependence of drain current variation on the IgE concentrations, the highest sensitivity of 290 pM was obtained, and sensor dissociation constant was estimated to be 47 nM. Since a variety of short peptide probes have been identified as biomarkers for many diseases,[16] graphene functionalized with these peptides noncovalently would enable the construction of graphene-based biosensors with excellent diagnostic function. However, all the above-discussed applications require specific adsorption configurations of biological molecules (proteins or peptides) to ensure the availability of one segment of the biomolecule to be solvent exposed, and simultaneously, the strong binding of another segment of the biomolecule to the graphene surface. To the best of our knowledge, there is very limited information about molecular interactions between biological molecules such as proteins and peptides and graphene, and how to control such interactions. Therefore, we believe that it is necessary to examine such interactions to better understand the molecular behaviors of proteins and peptides on graphene surfaces.

Theoretically, $\pi-\pi$ interactions (or stacking) between aromatic functionalities have been well recognized to be

Received: November 3, 2016
Published: January 16, 2017

DOI: 10.1021/jacs.6b11226
J. Am. Chem. Soc. 2017, 139, 1928−1936

important interactions between different peptide side chains, between side chain and backbone, and between peptide side chain and graphene surfaces.[17−22] A graphene surface has a composition that is dominantly planar aromatic and is expected to bind with peptide side chains with aromatic or amide groups.[17,23] Interestingly, all five independent all-atom simulation studies published previously reported strong binding affinity between a graphene surface and peptide side chains with planar groups.[24−28] Even though these results are not quantitatively comparable with each other, the deduced overall trends about the peptide side chain-graphene surface interactions are similar. With this knowledge in mind, we further tested the effect of $\pi-\pi$ interactions on interactions between peptide and graphene to understand peptide adsorption behavior and peptide orientation preference on a graphene surface. With such understanding, we hope that we are able to control peptide orientation on graphene by manipulating the peptide−graphene interaction through modification of the peptide sequence, improving the activity of the peptide molecules adsorbed on graphene. In order to understand how peptide sequence can affect binding and molecular orientation, two α-helical peptides with different distributions of hydrophilic residues were chosen. Cecropin P1 and MSI-78 both have planar side chains[17,23,29,30] throughout their peptide sequence, but have very different hydrophilic residue (especially lysine) distributions.

Surface sensitive techniques have been utilized to characterize peptides on graphene or graphite surfaces.[31−33] For instance, quartz crystal microgravimetry (QCM) has been applied to analyze the adsorption kinetics of peptides on graphene.[31] Optical techniques such as Raman spectroscopy and attenuated total reflection Fourier transform infrared (ATR-FTIR) spectroscopy were used to characterize peptide secondary structures by probing the amide I vibrational bands of peptides associated with graphene in dry conditions.[32,33] Scanning microscopic techniques (e.g., atomic force microscopy (AFM),[34−40] scanning tunneling microcopy (STM),[34,41] and high-resolution transmission electron microscopy (HR-TEM)[42,43]) have been used to obtain morphology of peptide adsorbed on both graphene and graphite surfaces in dry or solution conditions. It is worth noting that peptide−graphene interfacial interactions may be very different in dry versus in solution conditions. It is highly likely that the drying process strongly affects both secondary structure and orientation of peptides on graphene. In addition, peptide aggregation due to surface drying can result in alteration of the graphene surface morphology.[24] AFM[38−40] and STM[44] have been used to study liquid−solid interfaces and excellent results have been obtained. However, it can be challenging to use them to probe flexible structures (molecules are not completely bound to a substrate) due to the possible movements of the molecules under the probe tip.

For solution-based biosensors using peptides and graphene, it is expected that one end of the peptide interacts with and adsorbs onto the graphene surface, while the other end is solvent exposed, which is important for analyte binding in solution or ligand coupling to create extended materials.[7] Usually peptides interact with and adsorb on a graphene surface noncovalently. Since such noncovalent interaction/adsorption depends on a delicate balance of peptide-graphene, peptide−peptide, and peptide−solution interactions,[45] it is very challenging to accurately characterize peptide interaction/adsorption behavior on graphene in situ to determine peptide binding affinity with graphene and peptide orientation on graphene in solution. None of the above-discussed experimental studies[30−39] are able to reveal such details. Although molecular dynamics (MD) simulations have been used to elucidate the structure of peptides adsorbed on graphene or graphene oxide interfaces,[24−27,46] experimental results have not yet been reported to directly determine the secondary structure and orientation of peptides on graphene surface under aqueous conditions.

Sum frequency generation (SFG) vibrational spectroscopy[47−61] as a submonolayer surface and interface sensitive technique has great advantages in characterizing how peptides interact with and bind to graphene. Detailed structural information such as conformation and orientation of peptides on a graphene surface can be determined using SFG. SFG can selectively probe the amide I signal from peptides on graphene in situ in an aqueous environment; no background SFG signal is generated from the surrounding media which would interfere with peptide signal.[62] SFG signal is extremely sensitive to the ordering of peptides on graphene, and the dynamic information on peptide binding to graphene can be obtained by monitoring the SFG signal intensity change as a function of time. The secondary structure of peptides on a graphene surface can be probed by the SFG signal peak centers, and the orientation of peptides on graphene can be deduced by SFG signal strengths measured using different polarization combinations of the laser beams in the SFG experiment.[63,64] As mentioned above, here we chose two peptides that have very different hydrophilic and planar amino acid residue distributions to elucidate the effect of different amino acid residues on peptide−graphene interactions, and how such interactions influence peptide orientation on graphene. A combined experimental study using SFG and molecular dynamics (MD) simulations with a coarse grain model was performed.

2. MATERIALS AND METHODS

2.1. Materials. Graphene solution was purchased from Graphene Laboratories Inc. More details about the graphene samples can be found in the Supporting Information (SI). The pristine monolayer graphene flakes were dispersed in ethanol solution with a concentration of 1.0 mg/L. The C-terminus cysteine-modified cecropin P1 (CP1C, H_2N-SWLSKTAKKLENSAKKRISEGIAIAIQ-GGPRC—COOH, M_w = 3442 g/mol) was synthesized by Peptide 2.0 Inc. (Chantilly, VA). The N-terminus cysteine-modified MSI-78 (MSI-78(C1), CGIGKFLKKAKKFGKAFAKQLKK) and mutant MSI-78(C1) (CGIGK FLKKA KKAGK AAAKQ LKK) were synthesized by Professor Neil Marsh's group at the University of Michigan[65] and ordered from Peptide 2.0 Inc., respectively. Right-angle CaF_2 prisms were purchased from Altos Photonics (Bozeman, MT).

2.2. Graphene Sample Preparation. CaF_2 prisms were sonicated in ethanol and deionized water for 15 min each, and then were exposed to oxygen plasma for 3 min for cleaning. Ten μL of graphene solution (1 mg/L) was added onto one side of the right angle surface of the prism for graphene film deposition. After the graphene solution was completely dry, an AFM image was collected, showing that most of the CaF_2 surface was covered by monolayer graphene (Figure S1).[66] The graphene coated prism was then used for SFG experiment. For circular dichroism (CD) experiments, the sample preparation procedure is the same, except the use of high quality quartz slides instead of CaF_2 prisms for graphene deposition.

2.3. SFG Time-Dependent Measurements and SFG Spectra Collection. SFG theory and experimental details have been extensively reported[49,63,64,67,68] and will not be repeated here. In this study, SFG experiments were performed using a commercial SFG system from EKSPLA. Briefly the SFG system delivers picosecond (ps) laser pulses (20 ps pulse width) at a repetition rate of 50 Hz. One

DOI: 10.1021/jacs.6b11226
J. Am. Chem. Soc. 2017, 139, 1928−1936

pulse has a fixed wavelength at 532 nm, and the other pulse has tunable wavelength from 2.3 to 10 μm. The two pulses overlap spatially and temporally at the sample surface, then SFG signal can be collected. A near total reflection geometry was used for data collection, as discussed previously.[69−71] Peptide solution (0.5 μM) was placed in contact with the graphene coated CaF_2 prism from the bottom, and SFG signal was monitored as a function of time until equilibrium was reached. After the peptide solution was replaced several times using phosphate buffer (PB) solution (to wash off weakly adsorbed peptides), SFG spectra were collected with different polarization combinations of the input visible, input IR, and generated SFG beams, including ssp (s-polarized SFG signal, s-polarized visible input, and p-polarized input IR) and ppp.

2.4. Circular Dichroism (CD) Spectra Collection. The secondary structure of peptides adsorbed on graphene was measured by a J-1500 CD spectrometer (Jasco Inc., Japan) using a continuous scanning mode at room temperature. High quality quartz slides were used as substrates for CD experiments. Monolayer graphene coated quartz slides were immersed into the peptide solution (0.5 μM) for 30 min. After PB solution wash, a CD spectrum was collected between 240 and 190 nm at a 1 nm resolution and 50 nm/min scan rate, and averaged by five scans. To increase the CD signal, six slides with deposited graphene and adsorbed peptides were stacked together in the buffer solution and CD spectra were collected.

2.5. Simulation Method. *2.5.1. Graphene Surface Potential Model.* The coarse grained simulation method used in this work is based on a general solid surface force field developed previously,[72] which was built upon and incorporated with a well-known Karanicolas and Brooks (KB) Go-like protein model. The KB Go-like model has been shown in many cases to reproduce protein folding energy surfaces and folding mechanisms, which is an ideal model framework to study protein folding/adsorption energy surfaces at interfaces. With a well parametrized solid surface potential, this model has been successfully applied to several studies to understand and predict interfacial protein/peptide structures, stability, and orientations.[69,73−75] The parameters of this model were further optimized for room temperature applications as used in most cases.[76] This model quantitatively considered the attractive hydrophobic interactions between the protein/peptide residues and solid surfaces. In addition, the desolvation effect as an amino acid residue approaches the solid surface was also described in this model with a small energy barrier (by the third power term in eq 1).

As discussed above, the specific interactions between amino acid side-chains containing planar groups and the graphene surface may dominate the interactions when a peptide is adsorbed to a graphene surface as suggested by estimations of residue−graphene surface binding affinities.[24] To further extend the current coarse grained model to describe the graphene−residue interactions, in this work, we added an extra attractive term (by 2 units of hydrophobic index) to the seven amino acid residues with either an amide, aromatic, or guanidine group on their side chains (referred as "planar residues") to approximate the stacking (or $\pi-\pi$ interaction) effect in addition to the hydrophobic interactions between various residues and the graphene surface.[29] This value is chosen based on the average estimated value of the residue−graphene surface binding affinity reported in literature.[24−28]

We then have the graphene surface potential as follows:

$$V_{\text{graphene}} = \sum_{i}^{N} \left\{ \pi\rho\sigma_i^3\varepsilon_i \left[\theta_1 \left(\frac{\sigma_i}{z_{\text{is}}}\right)^9 - \theta_2 \left(\frac{\sigma_i}{z_{\text{is}}}\right)^7 + \theta_3 \left(\frac{\sigma_i}{z_{\text{is}}}\right)^3 - (\theta\chi_s + \theta_p(\chi_{\text{pi}} + 2\cdot\delta)) \left(\frac{\sigma_i}{z_{\text{is}}}\right)^3 \right] \right\} \quad (1)$$

where N is the residue number in the peptide, z_{is} is the distance between residue i and the graphene surface, σ_i and ε_i are residue specific van der Waals parameters. The parameters (θ's, Table S1) used in this work were determined in a previous study.[76]

The hydrophobic indices of the surfaces (χ_s, ranging from −1.0 to 4.5) and amino acids (χ_{pi}, ranging from −4.5 to 4.5) are used to differentiate surfaces and residues respectively, where a large positive number indicates hydrophobic and a negative number indicates hydrophilic. As in this case, the graphene surface has a relative hydrophobic property (water contact angle around 90°—see more discussions on the graphene surface hydrophobicity in the Conclusions section) with the χ_s set to be 1.5. The δ represents the Dirac delta function which equals to 1 for seven residues with "planar side-chains" (Arg, Trp, Phe, Tyr, His, Gln, and Asn) and 0 for all other residue types. There is disparity in the literature regarding the lysine-graphene binding affinity. Some studies suggest relatively strong affinity of lysine residues to graphene,[27,28] but others showed very weak binding.[24] Here we decided not to add an extra attractive term for the lysine interaction and follow the low binding free energy value for lysine as measured by Hughes et al.[24]

2.5.2. Molecular Dynamics Simulations. The peptide structures of cecropin P1 and MSI-78(C1) were constructed from their amino acid sequences with perfect α-helical structures. Each initial peptide structure was relaxed with energy minimization using CHARMM in implicit solvent. The relaxed structure was then submitted to the Go model builder on the MMTSB Web site (www.mmtsb.org) to generate an input file for the coarse grained simulation. Each peptide was initially positioned parallel to the graphene surface with a distance of about 10 Å above it as shown in Figure S3. For each peptide, three independent MD simulations were then performed within the canonical ensemble (NVT) at 298 K. Each simulation was performed with 10 million steps of equilibrium and 30 million steps of production with a time step of 5 fs. All-atom structures were reconstructed using the MMTSB tools (www.mmtsb.org) for visualization. Using the helical structures obtained from these simulations, we directly measured the helical content and helix orientation to the surface normal. With this data, the SFG $\chi^{(2)}_{zzz}/\chi^{(2)}_{yyz}$ ratio was calculated for each time frame and therefore the distribution of this ratio for the whole simulation trajectory was constructed. The detailed method used for calculation of the $\chi^{(2)}_{zzz}/\chi^{(2)}_{yyz}$ ratio is described in the SI. Specifically, the helical motif content in this small peptide was measured from the C_α-structures using a novel secondary structure assignment method PCASSO developed by Law et al.[77] This method is fast, efficient, and specific to C_α-only structures, which is an ideal method in analyzing structures calculated from the KB Go-like model.

2.5.3. MSI-78(C1) Peptide Mutation for Orientation Control. To evaluate the proposed mechanism of residue−graphene interaction and its effect on the peptide orientation, we performed a two-site mutation for the MSI-78 peptide with residues Phe 13 and 17 being replaced by Ala (F13A and F17A). Both mutation sites were chosen for the Phe residues to remove their strong adsorption to the surface due to $\pi-\pi$ interactions between the Phe side-chains and the graphene surface. Alanine residues are chosen for the mutant residues because they are slightly less hydrophobic than Phe, and they have strong propensity to form α-helical structures in the peptide.

3. RESULTS AND DISCUSSION

Peptide−graphene noncovalent interactions depend on the binding affinity of various residues in the peptide, and their distributions within the peptide sequence. Figure 1(a) shows cartoon images of cecropin P1 and MSI-78(C1). As we mentioned above, planar residue side chains, such as Arg17 and Arg31 (with the side chain colored in orange), Gln27 (yellow), Asn12 (red), and Trp2 (green) of cecropin P1 and Phe5, Phe12, and Phe16 of MSI-78(C1), have strong binding affinity to the graphene surface. The peptide−graphene noncovalent binding process was monitored by using time-dependent SFG measurements in a near total reflection geometry, as shown in Figure 1(b). Low concentration peptide solution (0.5 μM) was placed in contact with the graphene surface from below, and SFG signal was then measured as a function of time.

Figure 2(a) shows the change in SFG signal intensity for cecropin P1, illustrating the dynamic process of noncovalent binding to the graphene surface. The SFG signal of amide I (at

DOI: 10.1021/jacs.6b11226
J. Am. Chem. Soc. 2017, 139, 1928−1936

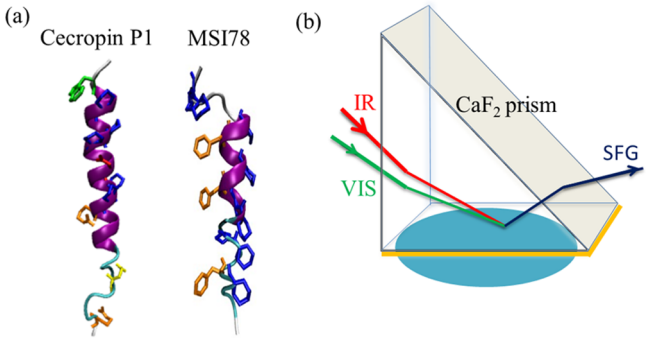

Figure 1. (a) Cartoon images of peptides cecropin P1 and MSI-78(C1). (b) Near-total reflection geometry for SFG spectra collection and time dependent SFG signal intensity measurement. The yellow layer represents the graphene surface and the peptide solution is drawn in light blue.

1650 cm^{-1}) increased gradually when cecropin P1 was added into the PB solution in contact with the graphene surface. This signal reached equilibrium after ~900 s. After replacing the peptide solution with PB buffer several times to wash loosely adsorbed peptides, SFG spectra were collected from cecropin P1 at the graphene/PB buffer interface with different input/output laser polarization combinations, as shown in Figure 2(b). Both ppp and ssp spectra show a strong amide I peak at ~1650 cm^{-1}, which is generated from the α-helical structure of cecropin P1 on the graphene surface. The SFG spectra were fitted using $|\chi^{(2)}|^2$ to obtain quantitative SFG signal strength and the fitting parameters are listed in Table S2. From these fitting results, we know $\chi^{(2)}_{ppp}/\chi^{(2)}_{ssp}$ = 1.42. After considering the influence of the Fresnel coefficient (~0.9), the $\chi^{(2)}_{zzz}/\chi^{(2)}_{yyz}$ ratio was deduced to be 1.58. This value can be used to determine the cecropin P1 orientation on the graphene surface, details of which are described in the SI.

Figure 2(c) shows time-dependent SFG signal collected after a solution of MSI-78(C1) was placed in contact with graphene to characterize the binding process of MSI-78(C1) to the graphene surface. Hardly any SFG signal was detected. SFG spectra were collected in the amide I frequency region but no discernible signal was detected (ssp spectrum is shown in Figure 2(d)). The absence of SFG signal could be the result of three possibilities: (i) No MSI-78(C1) was adsorbed to the graphene surface; (ii) MSI-78(C1) molecules were adsorbed onto the graphene surface, but the adsorbed peptides adopted a random structure (possessing an inversion symmetry at the interface) instead of α-helical structure; and (iii) MSI-78(C1) molecules were adsorbed onto the graphene surface and adopted the α-helical secondary structure, but lay down on the graphene surface. To determine whether MSI-78(C1) is able to bind to graphene and the secondary structure of the bound peptide on graphene (if any), CD spectra were measured from the interface between buffer washed graphene after contacting with MSI-78(C1) and PB buffer. If there is no peptide on the graphene surface, then the CD spectrum would be flat as the graphene reference spectrum. Also since CD spectra are

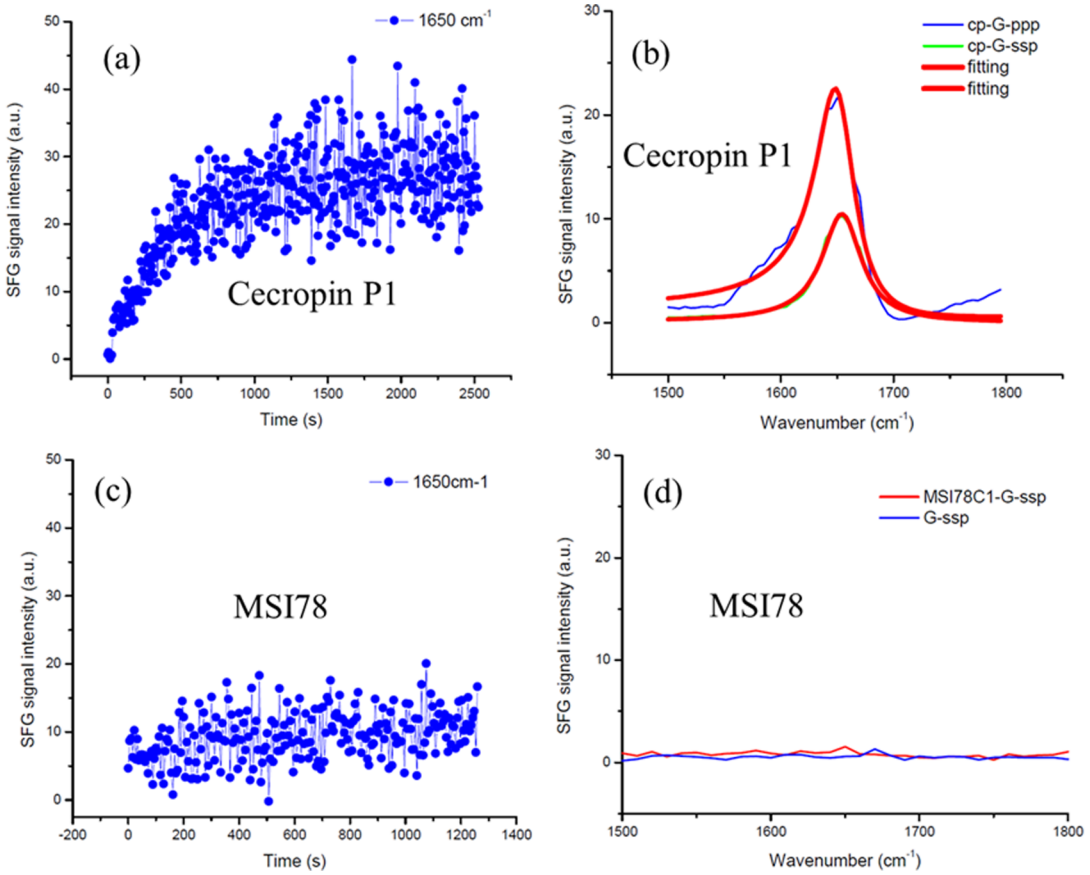

Figure 2. Kinetic information on the peptide–graphene interaction obtained by monitoring the time-dependent SFG signal of (a) cecropin P1 and (c) MSI-78(C1) after the peptide solution was placed in contact with graphene. (b) SFG data and the fitted results of cecropin P1 on graphene. (d) SFG spectra of MSI-78(C1) on graphene and graphene background.

DOI: 10.1021/jacs.6b11226
J. Am. Chem. Soc. 2017, 139, 1928–1936

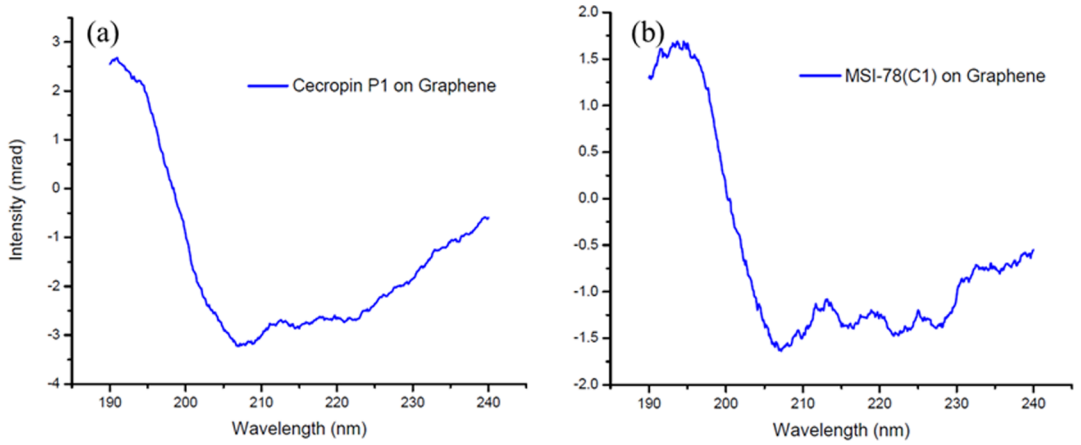

Figure 3. CD spectra of peptides cecropin P1 (a) and MSI-78(C1) (b) on a graphene surface.

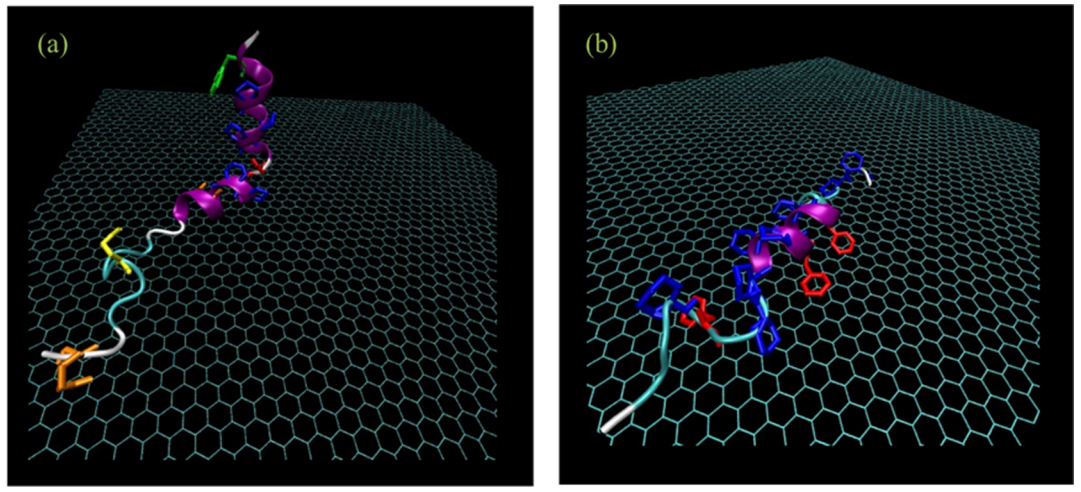

Figure 4. Molecular simulation results of peptide interactions with graphene. (a) Part of the cecropin P1 stands up and (b) MSI-78(C1) lies down on the graphene surface.

sensitive to peptide secondary structure, peptides adopting a random coil or α-helical structure is easily distinguished.

Figure 3 shows the CD spectra of cecropin P1 and MSI-78(C1) noncovalently binding with graphene. The spectra show negative peaks at 208 and 222 nm, indicating that both peptides cecropin P1 and MSI-78(C1) adopt an α-helical structure on the graphene surface.[69,71,75] Therefore, for MSI-78(C1) molecules, their CD data clearly indicate that they adsorb to the graphene surface adopting an α-helical structure. This shows that the absence of SFG signal detected from MSI-78(C1) on graphene is due to the fact that the peptide molecules are lying down on graphene. The combined SFG and CD studies showed very different interactions between graphene and the two peptides. Cecropin P1 has a standing up pose and MSI-78(C1) is lying down on the graphene surface. In the following, we will perform MD simulations to confirm the results obtained experimentally and to provide an in-depth understanding on the underline mechanisms of the peptide−graphene interactions for these two different peptides.

As shown in Figure 4, representative peptide structures of cecropin P1 and MSI-78(C1) were captured using coarse-grained MD simulations and the corresponding all-atom structures were reconstructed from the Cα conformation. Both structures were sampled near the end point of the simulation, each of which is representative both in secondary structure content and orientation on the graphene for all independent simulations. The helical structures are colored in purple in this representation. Planar residue side chains, to which we added extra adsorption energies are represented by lines and colored in orange for Arg17 and Arg31, yellow for Gln27, red for Asn12, and green for Trp2 in Figure 4(a) and red for Phe[5, 12, 16] in Figure 4(b). As discussed above, these residues were expected to bind strongly with the graphene surface. As shown in Figure 4(a), a large portion of cecropin P1 indeed lay down on the graphene surface, with a combination of the hydrophobic interactions and strong adsorption interactions between the planar side chains and the graphene surface. Arg17, Arg31, Asn12, and Gln27 were all adsorbed on the graphene as expected, but interestingly the Trp2 was found to be in the portion of the peptide helical structure that adopts a standing up conformation. A kink was detected at residue Asn12 between the two strands of helical structure. More importantly, we noticed that all the Lys residues (side chains shown in blue lines) are in the solvent-exposed segment of the peptide, which is believed to contribute largely to the specific conformation of this part of the peptide. In contrast, as shown in Figure 4(b), the whole peptide MSI-78(C1) was found to be completely lying down on the graphene. With a closer look, this peptide has a very balanced distribution of both the hydrophilic Lys residues (blue) and the Phe[5, 12, 16] residues (red) of

DOI: 10.1021/jacs.6b11226
J. Am. Chem. Soc. 2017, 139, 1928−1936

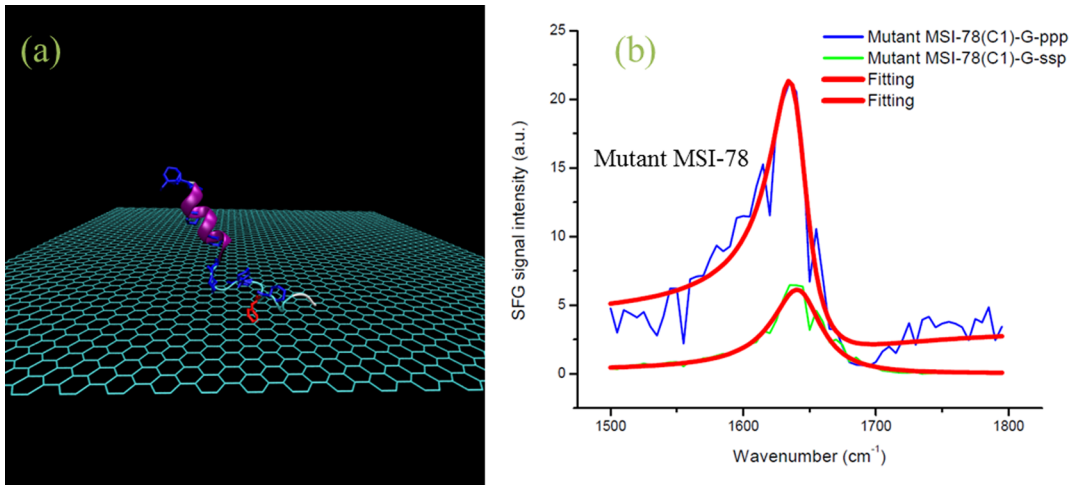

Figure 5. Molecular simulation results (a) and SFG spectra (b) of the mutant MSI-78(C1) peptide interactions with graphene.

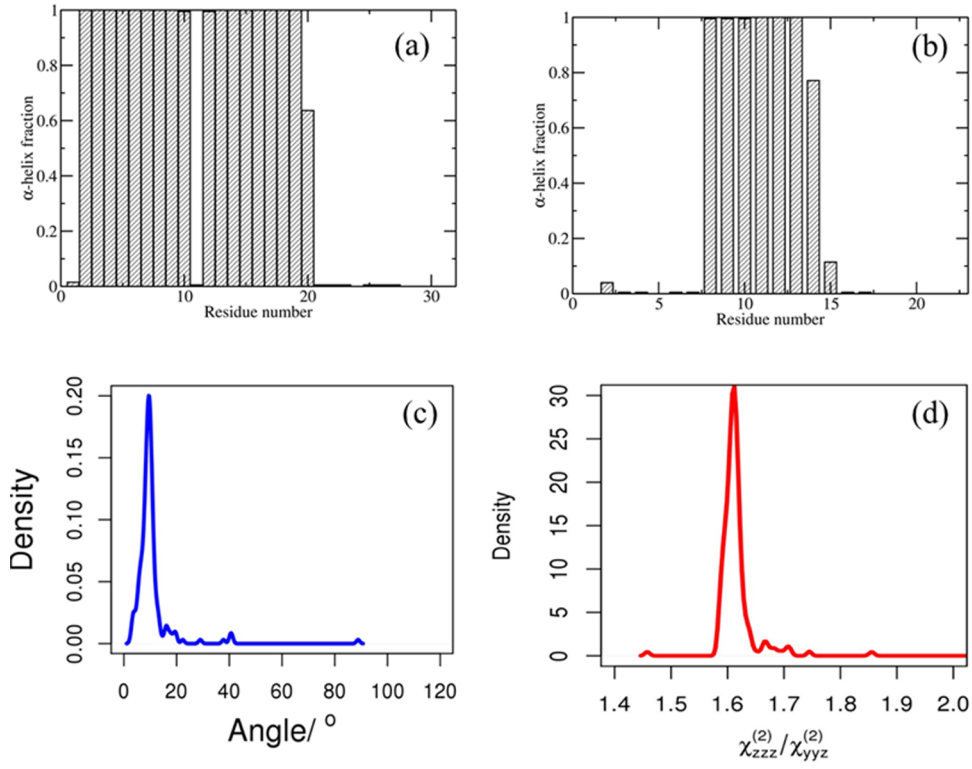

Figure 6. (a) Cecropin P1 and (b) MSI-78(C1) helical structure fraction for each residue on the graphene surface. (c) Orientation angle distributions of the cecropin P1 helical segment on graphene and (d) the calculated $\chi^{(2)}_{zzz}/\chi^{(2)}_{yyz}$ density distribution.

high-binding affinity throughout the whole peptide sequence. Therefore, the multiple Phe residues enable the entire peptide to lie down and the distributed Lys residues could not make a part of the peptide to stand up on the surface. Nevertheless, these observations from the MD simulations that a part of cecropin P1 stands up on the surface and MSI-78(C1) lies down completely are fully consistent with the experimentally measured results as shown above.

To make the peptide stand up on the graphene surface, a mutation was performed in the MSI-78(C1) peptide substituting two of the Phe residues to Ala (F13A and F17A). These mutation sites were chosen to break the observed balance of residue-graphene interactions throughout the peptide sequence. As a result of these mutations, the peptide exhibited a partially standing-up and partially flattened pose (Figure 5(a)). The adsorption was between the N-terminus of the peptide where the only remaining Phe residue exists, while the standing-up region is where we substituted Phe with Ala. Also, the standing-up region of the peptide formed a nice helical structure, which is achieved by choosing the high helical-structure propensity residues (Ala) for the mutant peptide. We then successfully validated the prediction from simulation experimentally. We applied SFG to study the interactions between mutant MSI-78(C1) peptides and graphene. SFG ssp and ppp amide I spectra were successfully collected from the interface between graphene and a MSI-78(C1) peptide solution (Figure 5(b)). The relative intensities of the ssp and ppp spectra show that the peptide adopts a standing up pose on

DOI: 10.1021/jacs.6b11226
J. Am. Chem. Soc. 2017, 139, 1928−1936

graphene. Both experimental and simulation studies carried out here demonstrated that mutating two aromatic amino acids with alanine could effectively reduce the peptide−graphene interaction, leading to a standing up pose for the peptide on graphene. Such a case study of a peptide mutation was performed to show that the proposed mechanism of residue−graphene interactions is reasonable, which has the potential to be applied in peptide/protein orientation control by peptide/protein sequence engineering.

For all the three cases, simulations were initiated with the peptide at the same distance above the graphene surface. Upon starting the simulation, the peptide adsorbed toward the surface. It was found that the N-terminus region of the peptide adsorbed to the graphene surface in a very stable way throughout the whole simulation. The average distances between the adsorbed amino acid residues and the graphene are identical (around 5 Å), which suggests the very similar potential energy for each residue−graphene interaction for the adsorbed residues for all three peptides.

As plotted in Figure 6(a,b), the secondary structure content was calculated from the MD simulations using the secondary structure estimator for the Cα conformations.[77] Cecropin P1 (Figure 6(a)) exhibited two segments of helical structure with a kink at residue Asn12. The MSI-78(C1) (Figure 6(b)) has a short segment of α-helix in the middle region of the sequence. We further evaluated the orientation of the small α-helical segment in cecropin P1 that stands up on the graphene surface using simulation. The tilt angle was measured for this helical segment vs the surface normal to be around 8° with a very narrow distribution (Figure 6(c)), suggesting a near-perpendicular pose for this part of cecropin P1 on the graphene surface. Using this peptide segment tilt angle and the helical structure length (10 residues), we calculated the SFG $\chi^{(2)}_{zzz}/\chi^{(2)}_{yyz}$ ratio distribution (Figure 6(d)). Consistent with the narrow tilt angle distribution, the calculated SFG $\chi^{(2)}_{zzz}/\chi^{(2)}_{yyz}$ ratio also exhibits a very narrow peak centered at around 1.6. This value matches the SFG experimental result of 1.58 (corresponding to a tilt angle of less than 10° shown in Figure S4) very well. Further, the simulation results of mutant MSI-78(C1) indicate the standing up helical segment has an average tilt angle of 32.8° vs the graphene surface normal, which is very close to the deduced tilt angle ∼30° from SFG experiment, as shown in Figure S5. Therefore, the results obtained from MD simulations reproduced the SFG measured peptide orientation and provided more detailed information on peptide structure on graphene. With the extra attraction term for seven different amino acid residues, we successfully modeled the effect of planar side chains on the peptide−graphene interaction along with the hydrophobic effects. Our MD simulation results indicate that the peptide orientation on graphene can be mediated by the position distribution of the planar side chain residues and the hydrophilic residues such as Lys.

4. CONCLUSIONS

In this research, we investigated the noncovalent interaction between two peptides and graphene in aqueous environment by SFG vibrational spectroscopy (supplemented by CD spectra) and coarse grained MD simulation. Different from previously reported research, here SFG allows us to monitor the peptide binding process to graphene in situ in real time, to characterize the peptide secondary structure on graphene, and to measure the peptide orientation on graphene. The MD simulation data matched the experimentally determined results quantitatively.

In this study we successfully tested our hypothesis that the peptide orientation on the graphene surface depends on the competition between the stacking interaction and interaction involving hydrophilic amino acid residues and the graphene surface. Our results showed that the unbalanced distribution of the hydrophilic/nonstacking lysine residues and the planar side chained residues is responsible for the partially standing-up pose of cecropin P1, while the evenly distributed planar side chains and hydrophilic residues led to the lying-down pose of MSI-78(C1). Knowledge of the competition effects between low and high graphene binding affinity residues would enable us to design peptides with particular sequence that could strongly interact with the graphene surface and stand up on the graphene surface. To do so, one peptide end should have enough residues with planar side chains to adsorb onto the graphene surface strongly, while the other peptide end should have hydrophilic residues so that they prefer to be away from the graphene surface (peptide stands up) to expose to aqueous solution. It is worth mentioning that in the literature, controversial results on the graphene surface hydrophobicity were reported.[78−82] We varied the graphene surface hydrophobicity in the range which was reported, similar results have been obtained in the simulations. Therefore, we believe that the results presented above in this article are reliable. This work sheds light on the development of strategies to control peptide−graphene noncovalent interaction and provides design rules to create peptides to stand up on a graphene surface. This is important for graphene based nanobio-medicine and nanobio-sensor development.

■ ASSOCIATED CONTENT

Supporting Information

The Supporting Information is available free of charge on the ACS Publications website at DOI: 10.1021/jacs.6b11226.

SFG data analysis, additional figures, MD simulation parameters, and SFG spectral fitting parameters (PDF)

■ AUTHOR INFORMATION

Corresponding Authors

*brookscl@umich.edu

*zhanc@umich.edu

ORCID

Xingquan Zou: 0000-0002-9716-9771

Minyu Xiao: 0000-0003-0083-4243

Charles L. Brooks III: 0000-0002-8149-5417

Author Contributions

The manuscript was written through contributions of all authors. All authors have given approval to the final version of the manuscript.

Author Contributions

[§]These authors contributed equally to this work.

Notes

The authors declare no competing financial interest.

■ ACKNOWLEDGMENTS

This research was supported by the Army Research Office (W911NF-11-1-0251) and National Science Foundation (CHE-1505385). The authors are grateful to Dr. Benjamin

DOI: 10.1021/jacs.6b11226
J. Am. Chem. Soc. 2017, 139, 1928−1936

Buer in Prof. Neil Marsh's group for synthesizing MSI-78(C1) peptides.

REFERENCES

(1) Castro Neto, A. H.; Guinea, F.; Peres, N. M. R.; Novoselov, K. S.; Geim, A. K. *Rev. Mod. Phys.* **2009**, *81*, 109.
(2) Geim, A. K. *Science* **2009**, *324*, 1530.
(3) Chung, C.; Kim, Y. K.; Shin, D.; Ryoo, S. R.; Hong, B. H.; Min, D. H. *Acc. Chem. Res.* **2013**, *46*, 2211.
(4) Ohno, Y.; Maehashi, K.; Matsumoto, K. *J. Am. Chem. Soc.* **2010**, *132*, 18012.
(5) Singh, M.; Holzinger, M.; Tabrizian, M.; Winters, S.; Berner, N. C.; Cosnier, S.; Duesberg, G. S. *J. Am. Chem. Soc.* **2015**, *137*, 2800.
(6) Chou, S. S.; De, M.; Luo, J. Y.; Rotello, V. M.; Huang, J. X.; Dravid, V. P. *J. Am. Chem. Soc.* **2012**, *134*, 16725.
(7) Russell, S. R.; Claridge, S. A. *Anal. Bioanal. Chem.* **2016**, *408*, 2649.
(8) Georgakilas, V.; Otyepka, M.; Bourlinos, A. B.; Chandra, V.; Kim, N.; Kemp, K. C.; Hobza, P.; Zboril, R.; Kim, K. S. *Chem. Rev.* **2012**, *112*, 6156.
(9) Feng, L. Y.; Wu, L.; Qu, X. G. *Adv. Mater.* **2013**, *25*, 168.
(10) Wang, Y.; Li, Z. H.; Wang, J.; Li, J. H.; Lin, Y. H. *Trends Biotechnol.* **2011**, *29*, 205.
(11) Bang, J. J.; Rupp, K. K.; Russell, S. R.; Choong, S. W.; Claridge, S. A. *J. Am. Chem. Soc.* **2016**, *138*, 4448.
(12) Mustata, G.-M.; Kim, Y. H.; Zhang, J.; DeGrado, W. F.; Grigoryan, G.; Wanunu, M. *Biophys. J.* **2016**, *110*, 2507.
(13) Mao, S.; Lu, G. H.; Yu, K. H.; Bo, Z.; Chen, J. H. *Adv. Mater.* **2010**, *22*, 3521.
(14) De, M.; Chou, S. S.; Dravid, V. P. *J. Am. Chem. Soc.* **2011**, *133*, 17524.
(15) Khatayevich, D.; Page, T.; Gresswell, C.; Hayamizu, Y.; Grady, W.; Sarikaya, M. *Small* **2014**, *10*, 1505.
(16) Soper, S. A.; Brown, K.; Ellington, A.; Frazier, B.; Garcia-Manero, G.; Gau, V.; Gutman, S. I.; Hayes, D. F.; Korte, B.; Landers, J. L.; Larson, D.; Ligler, F.; Majumdar, A.; Mascini, M.; Nolte, D.; Rosenzweig, Z.; Wang, J.; Wilson, D. *Biosens. Bioelectron.* **2006**, *21*, 1932.
(17) Flocco, M. M.; Mowbray, S. L. *J. Mol. Biol.* **1994**, *235*, 709.
(18) Hughes, Z. E.; Tomasio, S. M.; Walsh, T. R. *Nanoscale* **2014**, *6*, 5438.
(19) Duan, G.; Smith, V. H.; Weaver, D. F. *J. Phys. Chem. A* **2000**, *104*, 4521.
(20) Toth, G.; Watts, C. R.; Murphy, R. F.; Lovas, S. *Proteins: Struct., Funct., Genet.* **2001**, *43*, 373.
(21) McGaughey, G. B.; Gagne, M.; Rappe, A. K. *J. Biol. Chem.* **1998**, *273*, 15458.
(22) Burley, S. K.; Petsko, G. A. *Science* **1985**, *229*, 23.
(23) Bhattacharyya, R.; Saha, R. P.; Samanta, U.; Chakrabarti, P. *J. Proteome Res.* **2003**, *2*, 255.
(24) Hughes, Z. E.; Walsh, T. R. *J. Mater. Chem. B* **2015**, *3*, 3211.
(25) Pandey, R. B.; Kuang, Z. F.; Farmer, B. L.; Kim, S. S.; Naik, R. R. *Soft Matter* **2012**, *8*, 9101.
(26) Camden, A. N.; Barr, S. A.; Berry, R. J. *J. Phys. Chem. B* **2013**, *117*, 10691.
(27) Dragneva, N.; Floriano, W. B.; Stauffer, D.; Mawhinney, R. C.; Fanchini, G.; Rubel, O. *J. Chem. Phys.* **2013**, *139*, 174711.
(28) Welch, C. M.; Camden, A. N.; Barr, S. A.; Leuty, G. M.; Kedziora, G. S.; Berry, R. J. *J. Chem. Phys.* **2015**, *143*, 045104.
(29) Hooft, R. W. W.; Sander, C.; Vriend, G. *J. Appl. Crystallogr.* **1996**, *29*, 714.
(30) Brocchieri, L.; Karlin, S. *Proc. Natl. Acad. Sci. U. S. A.* **1994**, *91*, 9297.
(31) Kim, S. S.; Kuang, Z. F.; Ngo, Y. H.; Farmer, B. L.; Naik, R. R. *ACS Appl. Mater. Interfaces* **2015**, *7*, 20447.
(32) Katoch, J.; Kim, S. N.; Kuang, Z. F.; Farmer, B. L.; Naik, R. R.; Tatulian, S. A.; Ishigami, M. *Nano Lett.* **2012**, *12*, 2342.
(33) Han, T. H.; Lee, W. J.; Lee, D. H.; Kim, J. E.; Choi, E. Y.; Kim, S. O. *Adv. Mater.* **2010**, *22*, 2060.
(34) Claridge, S. A.; Thomas, J. C.; Silverman, M. A.; Schwartz, J. J.; Yang, Y. L.; Wang, C.; Weiss, P. S. *J. Am. Chem. Soc.* **2013**, *135*, 18528.
(35) Kim, S. N.; Kuang, Z. F.; Slocik, J. M.; Jones, S. E.; Cui, Y.; Farmer, B. L.; McAlpine, M. C.; Naik, R. R. *J. Am. Chem. Soc.* **2011**, *133*, 14480.
(36) Cui, Y.; Kim, S. N.; Jones, S. E.; Wissler, L. L.; Naik, R. R.; McAlpine, M. C. *Nano Lett.* **2010**, *10*, 4559.
(37) So, C. R.; Hayamizu, Y.; Yazici, H.; Gresswell, C.; Khatayevich, D.; Tamerler, C.; Sarikaya, M. *ACS Nano* **2012**, *6*, 1648.
(38) Yu, X.; Wang, Q. M.; Lin, Y. A.; Zhao, J.; Zhao, C.; Zheng, J. *Langmuir* **2012**, *28*, 6595.
(39) Prokhorov, V. V.; Klinov, D. V.; Chinarev, A. A.; Tuzikov, A. B.; Gorokhova, I. V.; Bovin, N. V. *Langmuir* **2011**, *27*, 5879.
(40) Jordens, S.; Riley, E. E.; Usov, I.; Isa, L.; Olmsted, P. D.; Mezzenga, R. *ACS Nano* **2014**, *8*, 11071.
(41) Mao, X. B.; Guo, Y. Y.; Luo, Y.; Niu, L.; Liu, L.; Ma, X. J.; Wang, H. B.; Yang, Y. L.; Wei, G. H.; Wang, C. *J. Am. Chem. Soc.* **2013**, *135*, 2181.
(42) Li, C. X.; Adamcik, J.; Mezzenga, R. *Nat. Nanotechnol.* **2012**, *7*, 421.
(43) Wilson, N. R.; Pandey, P. A.; Beanland, R.; Young, R. J.; Kinloch, I. A.; Gong, L.; Liu, Z.; Suenaga, K.; Rourke, J. P.; York, S. J.; Sloan, J. *ACS Nano* **2009**, *3*, 2547.
(44) De Feyter, S.; De Schryver, F. C. *J. Phys. Chem. B* **2005**, *109*, 4290.
(45) MacLeod, J. M.; Rosei, F. *Small* **2014**, *10*, 1038.
(46) Mijajlovic, M.; Penna, M. J.; Biggs, M. J. *Langmuir* **2013**, *29*, 2919.
(47) Shen, Y. R. *Nature* **1989**, *337*, 519.
(48) Richmond, G. L. *Chem. Rev.* **2002**, *102*, 2693.
(49) Chen, Z.; Shen, Y. R.; Somorjai, G. A. *Annu. Rev. Phys. Chem.* **2002**, *53*, 437.
(50) Su, Y. D.; Han, H. L.; Cai, Q.; Wu, Q.; Xie, M. X.; Chen, D. Y.; Geng, B. S.; Zhang, Y. B.; Wang, F.; Shen, Y. R.; Tian, C. S. *Nano Lett.* **2015**, *15*, 6501.
(51) Chen, X.; Yang, T.; Kataoka, S.; Cremer, P. S. *J. Am. Chem. Soc.* **2007**, *129*, 12272.
(52) Flores, S. C.; Kherb, J.; Cremer, P. S. *J. Phys. Chem. C* **2012**, *116*, 14408.
(53) Chen, X.; Sagle, L. B.; Cremer, P. S. *J. Am. Chem. Soc.* **2007**, *129*, 15104.
(54) Horowitz, Y.; Han, H. L.; Ross, P. N.; Somorjai, G. A. *J. Am. Chem. Soc.* **2016**, *138*, 726.
(55) Hsieh, C. S.; Campen, R. K.; Verde, A. C. V.; Bolhuis, P.; Nienhuys, H. K.; Bonn, M. *Phys. Rev. Lett.* **2011**, *107*, 116102.
(56) Weidner, T.; Castner, D. G. *Phys. Chem. Chem. Phys.* **2013**, *15*, 12516.
(57) Lovering, K. A.; Bertram, A. K.; Chou, K. C. *J. Phys. Chem. C* **2016**, *120*, 18099.
(58) Covert, P. A.; Hore, D. K. *J. Phys. Chem. C* **2015**, *119*, 271.
(59) Ye, S.; Tong, Y. J.; Ge, A. M.; Qiao, L.; Davies, P. B. *Chem. Rec.* **2014**, *14*, 791.
(60) Huang, J. H.; Tian, K. Z.; Ye, S. J.; Luo, Y. *J. Phys. Chem. C* **2016**, *120*, 15322.
(61) Wang, Z. G.; Morales-Acosta, M. D.; Li, S. H.; Liu, W.; Kanai, T.; Liu, Y. T.; Chen, Y. N.; Walker, F. J.; Ahn, C. H.; Leblanc, R. M.; Yan, E. C. Y. *Chem. Commun.* **2016**, *52*, 2956.
(62) Haupert, L. M.; Simpson, G. J. *Annu. Rev. Phys. Chem.* **2009**, *60*, 345.
(63) Nguyen, K. T.; Le Clair, S. V.; Ye, S.; Chen, Z. *J. Phys. Chem. B* **2009**, *113*, 12169.
(64) Wang, J.; Lee, S. H.; Chen, Z. *J. Phys. Chem. B* **2008**, *112*, 2281.
(65) Jasensky, J. Ph.D. Thesis, The University of Michigan, 2015.
(66) Gupta, A.; Chen, G.; Joshi, P.; Tadigadapa, S.; Eklund, P. C. *Nano Lett.* **2006**, *6*, 2667.
(67) Zhuang, X.; Miranda, P. B.; Kim, D.; Shen, Y. R. *Phys. Rev. B: Condens. Matter Mater. Phys.* **1999**, *59*, 12632.
(68) Moad, A. J.; Simpson, G. J. *J. Phys. Chem. B* **2004**, *108*, 3548.

DOI: 10.1021/jacs.6b11226
J. Am. Chem. Soc. 2017, 139, 1928−1936

(69) Wang, Q. M.; Wei, S.; Wu, J. F.; Zou, X. Q.; Sieggreen, O.; Liu, Y. W.; Xi, C. W.; Brooks, C. L., III; Chen, Z. *J. Phys. Chem. C* **2015**, *119*, 22542.
(70) Li, Y. X.; Zhang, X. X.; Myers, J.; Abbott, N. L.; Chen, Z. *Chem. Commun.* **2015**, *51*, 11015.
(71) Wei, S.; Zou, X.; Cheng, K.; Jasensky, J.; Wang, Q.; Li, Y.; Hussal, C.; Lahann, J.; Brooks, C. L., III; Chen, Z. *J. Phys. Chem. C* **2016**, *120*, 19078.
(72) Wei, S.; Knotts, T. A. *J. Chem. Phys.* **2013**, *139*, 095102.
(73) Ogorzalek, T. L.; Wei, S.; Liu, Y. W.; Wang, Q. M.; Brooks, C. L., III; Chen, Z.; Marsh, E. N. G. *Langmuir* **2015**, *31*, 6145.
(74) Wei, S.; Brooks, C. L., III *Chin. Chem. Lett.* **2015**, *26*, 485.
(75) Li, Y. X.; Wei, S.; Wu, J. F.; Jasensky, J.; Xi, C. W.; Li, H. L.; Xu, Y. M.; Wang, Q.; Marsh, E. N. G.; Brooks, C. L., III; Chen, Z. *J. Phys. Chem. C* **2015**, *119*, 7146.
(76) Wei, S.; Logan, S. A.; Brooks, C. L., III *Submitted*, 2016
(77) Law, S. M.; Frank, A. T.; Brooks, C. L., III *J. Comput. Chem.* **2014**, *35*, 1757.
(78) Li, Z. T.; Wang, Y. J.; Kozbial, A.; Shenoy, G.; Zhou, F.; McGinley, R.; Ireland, P.; Morganstein, B.; Kunkel, A.; Surwade, S. P.; Li, L.; Liu, H. T. *Nat. Mater.* **2013**, *12*, 925.
(79) Rafiee, J.; Mi, X.; Gullapalli, H.; Thomas, A. V.; Yavari, F.; Shi, Y. F.; Ajayan, P. M.; Koratkar, N. A. *Nat. Mater.* **2012**, *11*, 217.
(80) Shih, C. J.; Wang, Q. H.; Lin, S. C.; Park, K. C.; Jin, Z.; Strano, M. S.; Blankschtein, D. *Phys. Rev. Lett.* **2012**, *109*, 176101.
(81) Raj, R.; Maroo, S. C.; Wang, E. N. *Nano Lett.* **2013**, *13*, 1509.
(82) Kim, D.; Pugno, N. M.; Buehler, M. J.; Ryu, S. *Sci. Rep.* **2015**, *5*, 15526.

DOI: 10.1021/jacs.6b11226
J. Am. Chem. Soc. 2017, 139, 1928−1936